JOURNAL OF MATERIALS SCIENCE 33 (1998) 3805–3816

Microstructural inhomogeneities and sea water corrosion in laser-deposited Ti–6Al–4V alloy matrix/carbide particulate composite surfaces

K. P. COOPER, P. L. SLEBODNICK
Materials Science and Technology Division, Naval Research Laboratory, Washington, DC 20375, USA
E-mail: cooper@anvil.nrl.navy.mil

K. E. LUCAS
Marine Corrosion Facility, Naval Research Laboratory, Key West, FL 33040, USA

E. A. HOGAN
Geo-Centers, Inc., Fort Washington, MD 20744, USA

Metal matrix/carbide particulate composite surface layers were produced on Ti–6Al–4V alloy samples by injecting metal carbide particles into laser-melted surfaces followed by rapid solidification. Hard, wear-resistant surfaces were produced on a strong alloy which normally has poor wear resistance. The corrosion behaviour of the composite surface was evaluated after a month's exposure to flowing sea water. A variety of solidification products was found in the laser-deposited surface layers, but corrosion was observed only in the carbide particulate phase in the WC-injected sample. No corrosion was observed in the TiC-injected sample nor in the Ti–6Al–4V base alloy. Corrosion in the WC-injected sample was related to the formation of a narrow interphase zone surrounding the particulate phase and a thin reaction zone on the surface of the particulate phase during solidification. The titanium-rich interphase zone formed a galvanic couple with the WC particulate. Crevice-type corrosion initiated at the interface between the two phases and proceeded into the particulate phase assisted by the reaction zone. Electrochemical test results revealed a high corrosion rate for the WC-injected sample and almost none for both the TiC-injected sample and the Ti–6A1–4V base alloy, confirming the microstructural observations.

1. Introduction

Surface modification involving particulate/metal matrix composite structures produces materials with very high hardness and improved wear resistance. Among several techniques for forming such coatings, laser surface treatment has shown considerable promise [1, 2]. The laser is a source of energy that is chemically clean and that can be delivered in precise quantities. Laser melting results in a strong metallurgical bond between the fusion zone and the substrate. The rapid self-quenching produces a narrow heat-affected zone (HAZ), low workpiece distortion and fine-scale microstructures exhibiting superior mechanical properties. The laser is easily manoeuvrable and suited for automation, making possible the processing of selected areas and confined locations such as valve seats, piston grooves and shaft seal faces, saving on cost and deterioration of bulk properties. Particulate/metal matrix composite surface layers can be made by laser melt/particle injection in which hard particles such as carbides are impregnated into a laser melt pool formed on the substrate surface [3, 4]. The increase in hardness and wear resistance is primarily due to particulate reinforcement of the metal matrix and resistance to plastic flow by the particulates during wear and abrasion. Secondary contributions to improved hardness and wear resistance can come from solidification reaction products such as fine-scale, dendritic and eutectic carbides that form within the metal matrix as a result of melt/carbide interactions, and from phase transformation products such as solid solutions, precipitates, dispersoids, and martensitic phases [3, 4].

Usually, components surface treated for wear resistance are used in non-aggressive environment. However, in the drive to design economical systems, components are finding more use in harsh environments. For example, the US Navy is interested in materials that exhibit both superior wear resistance and superior corrosion resistance. Unfortunately, the same microstructural changes that enhance wear resistance can adversely affect corrosion resistance. For

example, bonded wear-resistant cladding is necessarily made of a material different from the base metal, thereby opening up the possibility of galvanic corrosion at the bond. In some cases, the overlay itself has poor resistance to corrosion in many environments. Laser melt/ particle injection processing strives to retain the inherent properties of the material while enhancing its wear resistance. The metal matrix is similar in chemistry to the substrate and should exhibit properties similar to it. In addition, most metal carbides have very good corrosion resistance. However, an earlier sea water corrosion study [5] of Inconel 625 alloy with WC and TiC injected surfaces found different degrees of corrosion in different regions of the laser-deposited surface layers. It also found that the corrosion resistance of the TiC-injected sample was superior to that of the WC-injected sample. In that alloy, corrosion occurred as a result of the partitioning of useful corrosion inhibitors such as chromium, molybdenum and niobium out of solution during processing, and of the formation of galvanic microcells between the various solidification species and the metal matrix. It is important to understand the corrosion behaviour of the reinforcement phase because its loss would destroy its ability to enhance wear resistance. This study examined and evaluated microstructural inhomogeneities and sea water corrosion of carbide-reinforced Ti–6Al–4V alloy which is of interest to the US Navy because of increased use of titanium alloys in valve materials and as replacements for Monels (Cu–Ni alloys).

2. Experimental procedure

2.1. Laser processing and solidification structure

Carbide particulate/metal matrix composite surface layers were laser-deposited on 0.625 cm thick, 10 cm^2 hot-rolled Ti–6Al–4V alloy coupons. Using optimum processing conditions, two sample coupons were fabricated. One was injected with WC and the other with TiC. With a high-power CW, CO_2 laser beam, a shallow melt pool was formed on the sample surface. Into this melt pool were injected 45–75 μm carbide particles propelled by helium carrier gas. Processing was done in a chamber that was evacuated and back-filled with helium, thereby minimizing contamination. The laser power density of 20–30 kW cm^{-2} was high enough to produce a desired amount of melt but insufficient to melt or fuse the higher melting point carbide particles. As the sample was traversed under the laser beam and injection nozzle, a strip of injected layer was formed. The injected layer was 0.1–0.2 cm thick, 0.3–0.4 cm wide and was uniformly loaded with about 50 vol% carbide particulate. The samples were sectioned, mounted and polished with diamond paste to a 1 μm finish. Prior to corrosion testing, the unetched samples were examined in a Hitachi Model S-800 Field Emission scanning electron microscope (SEM) and evaluated for microstructure. In the WC-injected sample, the atomic number contrast was sufficient to identify the various phases in the microstructure using the secondary electron imaging mode. Tungsten-rich phases were of light contrast, titanium-rich phases were of dark contrast. Phase identification, extent of alloying and segregation were determined using standard line scan techniques available with the Princeton Gamma-Tech energy dispersive spectrometer (EDS) analysis system. Because the microstructural features were fine-scale, the resolution of the EDS technique was not sufficient for quantitative analysis. Nor was it possible to resolve the lower concentration elements aluminium and vanadium. However, this method did provide a good qualitative sense for the chemical distribution of the major elements tungsten and titanium in the various phases. Detailed microstructural analysis of the as-processed samples was performed to characterize the extent of microstructural inhomogeneity in the modified layer and to identify regions that could be susceptible to corrosion.

2.2. Corrosion tests

For the sea water corrosion test, the as-polished samples were suspended in gently flowing, natural, unfiltered sea water at NRL's Marine Corrosion Facility at Key West, FL, USA over a period of 1 mon. Details of the test were given in a previous paper [5]. After exposure, the samples were removed and cleaned, first in distilled water and then in alcohol to remove any loosely adhering sludge. The cleaned samples were examined in the SEM for the type and extent of corrosion. Corrosion rates of the laser-deposited layers and of the base metal were determined using electrochemical polarization resistance measurement techniques and Tafel slope analysis. The electrochemical equipment for these tests consisted of a 4 l container filled with natural sea water. It was a once-through system with the sea water refreshed at an approximate rate of 100 ml min^{-1}. Sea water parameters are given in Table I. A platinum mesh basket counter electrode was placed 10 cm from a working electrode surface and a Ag/AgCl reference cell was placed within 1 mm of the working electrode. Because the test specimens were mounted in standard metallurgical mounts, electrical connection was established by tapping a hole in the epoxy mount and tightening a screw securely against the metal specimen. Once a good low-resistance contact was achieved, the screw and associated wire were potted off to insulate the connection. The specimen surface was then masked with Glyptol™ to isolate the laser-deposited area of the specimen from the base metal area for testing. The sample was placed in the electrolyte and the potential was allowed to stabilize for approximately 1 h before running the polarization scans. A scan rate of 0.1 mV s^{-1} was used and the exposed area was about 0.1 cm^2.

TABLE I Seawater parameters for electrochemical test

Temperature	25.7 °C
Salinity	35.5 g kg^{-1}
pH	8.05
Dissolved O_2	6.37 mg l^{-1}
Resistivity	18.7 Ω cm

Measurements were taken using an EG and G Princeton Applied Research Model 273 potentiostat.

3. Results

3.1. Microstructural analysis of solidification structure

The laser-deposited surface layer consisted of uniformly distributed carbide particles in a metal matrix. While the carbide particulates were mostly unaltered in their internal structure during the processing, a variety of product phases formed within the metal matrix. The microstructure in Fig. 1a is of a region near the substrate/injected layer interface in the WC-injected sample and it shows the substrate (S), the metal matrix (M) and the carbide (C). Fig. 1b gives the line scans of tungsten (shaded area) and titanium (scattered dots) across the interface which show pick-up of a small

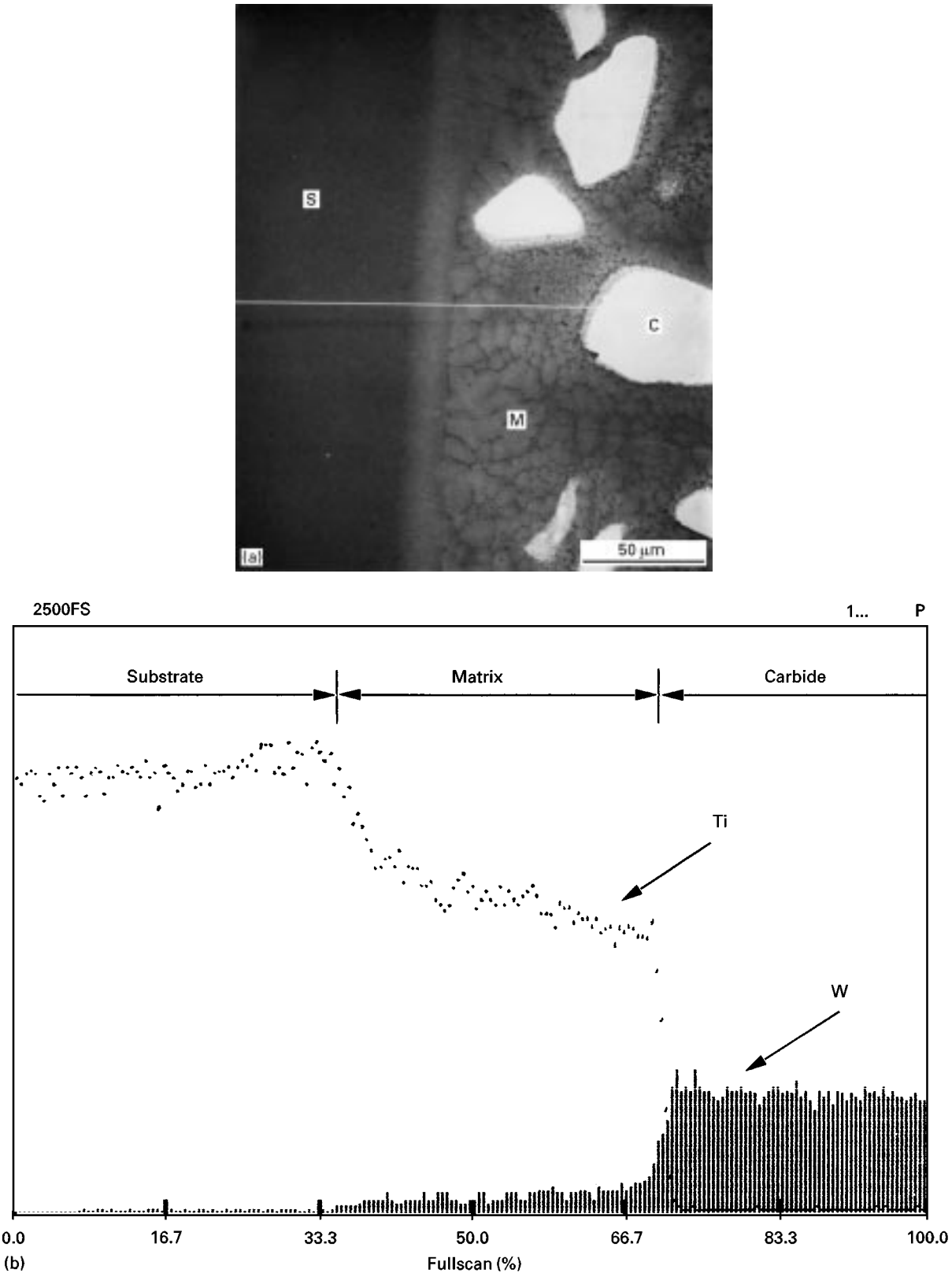

Figure 1 (a) Microstructure of substrate/injected layer interface region in a WC-injected Ti–6Al–4V sample showing substrate (S), matrix (M) and carbide (C). (b) Corresponding line scan showing tungsten pick-up in the matrix phase.

amount of tungsten in the Ti–6Al–4V alloy matrix. The metal matrix solidifies with a cellular structure as shown in Fig. 2a, with a fine-scale eutectic mixture (E) decorating the cell boundaries. In the upper regions of the injected layer, a dispersion of dendrites (D) was observed as shown in Fig. 2b. These dendrites are in dark contrast, meaning that they were probably rich in titanium. This was confirmed by the line scan in Fig. 3a, taken across the dendrite in Fig. 3b, which shows enhanced titanium and depleted tungsten within the dendrite compared to the surrounding matrix. Another solidification product is an interphase zone around the WC particulates. The interphase zone (IZ) appears as a continuous 1–2 μm thick film as shown in Fig. 4. A close-up of the interphase zone revealed a cellular-dendritic morphology as shown in Fig. 5a. The interphase zone is of dark contrast, suggesting that it is probably rich in titanium. This was confirmed by the line scan shown in Fig. 5b which shows enhanced titanium and depleted tungsten in the interphase zone. In Fig. 5a, the edge of the WC particulate appears pitted over a micrometre thickness. This pitted zone, which was found only in the carbide phase, probably resulted from a reaction between the carbide and the melt and was observed to vary in size. An extreme example of this reaction zone (RZ) is shown in Fig. 6a. It is about 3 μm thick. A line scan across this micrograph appears in Fig. 6b, and it clearly shows in the reaction zone an "infiltration" of titanium and a depletion of tungsten compared to the rest of the carbide particulate. Also observed in the solidified structure was porosity scattered within the matrix phase.

In the TiC-injected sample, the metal matrix was slightly enriched in titanium which was confirmed by a line scan, not reproduced here, across the substrate/injected layer interface. As was the case with the WC-injected sample, the matrix phase in the TiC-injected layer solidified with a cellular structure with intercellular eutectic (E) as shown in Fig. 7a taken near the substrate/injected layer interface. In the upper regions of the injected layer, a network-type, dendritic (D) structure formed in the matrix phase as shown in Fig. 7b. This structure appears similar to the network-type dendrites observed in TiC-injected Inconel 625 alloy [5]. Absent in the TiC-injected layers were any interphase zone, reaction zone and dispersed porosity that were found in the WC injected layer.

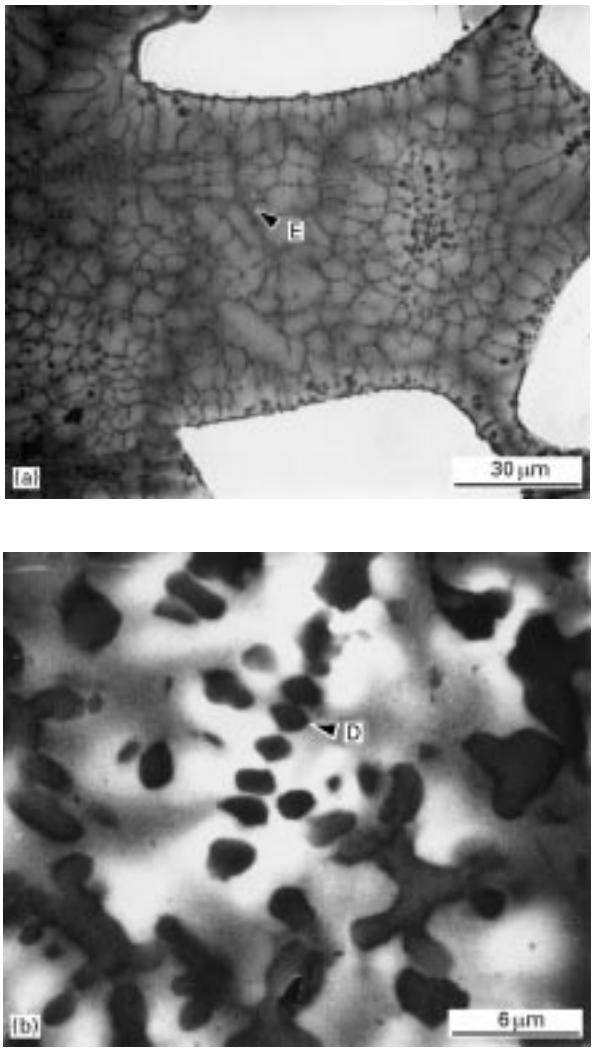

Figure 2 (a) Cellular metal matrix microstructure in a WC-injected sample with inter-cellular eutectic mixture (E). (b) Dendritic phase (D) found in the upper regions of the injected layer.

3.2. Microstructural analysis after sea water exposure

Crevice-type corrosion was observed in the WC-injected sample at the boundary (A) between the carbide particulate (C) and the interphase zone (IZ) as shown in Fig. 8. The attacked region was narrow and deep. Careful examination of the microstructure revealed that the corrosion was on the carbide side and not on the interphase zone side. Also observed was corrosion across the exposed polished surface of the carbide particulate which gave it a rough appearance as shown in Fig. 8. Corrosion across the particulate phase occurred to different degrees. In Fig. 9a, the carbide particle on the right shows crevice-type corrosion along the interface and roughening of the surface. On the other hand, the cavity in the top left of the same micrograph resulted from the complete dissolution of a carbide particle. Many particles were partially dissolved such as that shown in Fig. 9b. Close examination of the region near the crevice of several modestly corroded WC particulates revealed no trace of the reaction zone that was around the particulate edge. An examination of the matrix phase revealed the total absence of corrosion within it. A comparison of the matrix in Fig. 8 with that in Fig. 2a shows no corrosion in the tungsten-alloyed cellular structure, nor in or near the inter-cellular titanium-rich eutectic phase. A comparison of the matrix in Fig. 10 with that in Fig. 2b shows no corrosion in or near the titanium-rich dendritic carbide structure. The pore in Fig. 11 shows only the as-solidified intercellular eutectic carbide structure and no corrosion. The absence of corrosion in the TiC injected sample was demonstrated by comparing the micrographs in Fig. 12a and b with identical micrographs in Fig. 7a and b, respectively. No corrosion was observed in or near the eutectic phase, nor in or near the dendritic phase, nor at the particulate/metal matrix boundary.

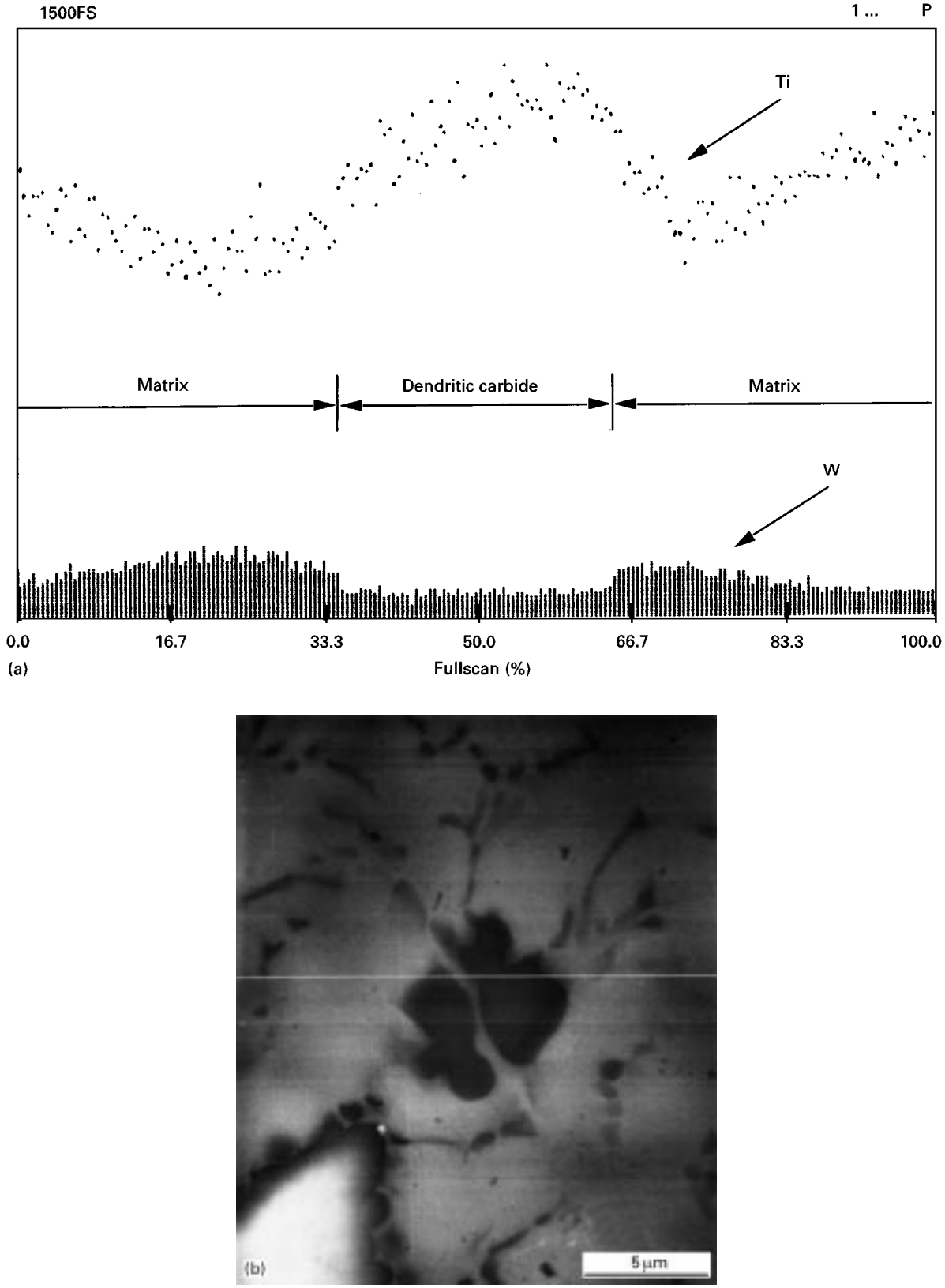

Figure 3 (a) Line scan showing increased titanium in the dendritic phase in WC-injected sample. (b) Corresponding microstructure.

3.3. Corrosion rate measurements

Polarization curves for the (a) Ti–6Al–4V base alloy, the (b) WC-injected layer and the (c) TiC-injected layer are given in Fig. 13. For the carbide-injected layers, the anodic curves exhibit evidence of a secondary reaction located at potentials near 30 mV versus Ag/AgCl reference electrode and greater than 150 mV anodic with respect to $I = 0$. The computer-calculated corrosion rates are summarized in Table II. Corrosion rates were determined from the data extracted from the electrochemical polarization behaviour and from subsequent electrochemical calculations using the polarization resistance method and Tafel slope analysis. The WC-injected sample had a higher corrosion rate

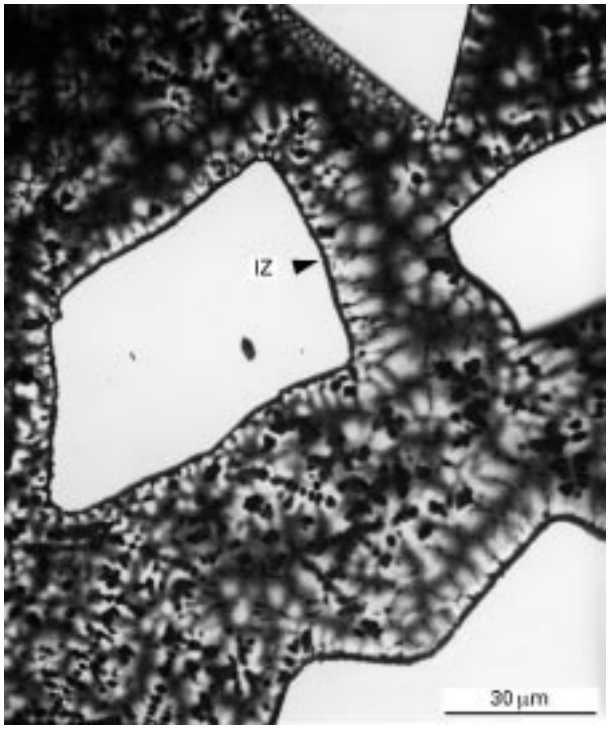

Figure 4 Microstructure showing interphase zone (IZ) surrounding the particulates in the WC-injected sample.

than the TiC-injected sample and the base alloy. There is agreement between the polarization resistance and Tafel analysis methods except in the case of the Ti–6Al–4V base alloy.

4. Discussion

The microstructure of the as-received Ti–6Al–4V alloy plate consisted of an α-rich, α + β phase mixture. Laser melting with particle injection resulted in a structure that had uniformly dispersed carbide particles in an alloy matrix that was similar in composition, but not in microstructure, to the base metal. Owing to mixing in the melt pool and to the high melt temperatures, partial dissolution of the carbide particulates into the melt occurred. The result was enrichment of the melt in carbon and tungsten or titanium, depending upon the injected species. Upon solidification of the enriched melt, a variety of product phases formed. Because carbon is one of the dissolved elements, these resolidification products were most likely carbides. Enhanced microhardness of the matrix from dispersion hardening also suggested that these product phases may be carbides [4]. Even as solidification initiated at the substrate, heavily alloyed dendritic carbides precipitated out of the supersaturated melt ahead of the growth front. These high-melting point dendritic carbides formed in the hotter, upper regions of the melt pool in places where there were high concentrations of the dissolved species. Owing to the rapid growth rates, the remainder of the melt solidified with a cellular structure around the dendritic carbides and the carbide particulates. As the last liquid was enriched in solute elements such as carbon, it solidified in the inter-cellular regions as fine-scale eutectic carbides. Owing to the rapid quench, the matrix phase is most likely martensitic. It is well-known that quenching of Ti–6Al–4V from 1010 °C or above produces martensite-like microstructures [6]. Microhardness data of regions in the matrix phase free of dendritic carbides matched that of the HAZ which was martensitic [4].

In the WC-injected sample, the diffusional exchange of tungsten and titanium at the boundary between the WC particulate and the titanium alloy liquid metal resulted in the formation of an interphase zone on the matrix side and a reaction zone on the particulate side. The interphase zone appears similar to the dendritic carbides. It is titanium rich, cellular–dendritic, and is of dark contrast. Thus, we infer that the interphase zone is also a carbide and formed before solidification of the liquid metal around the particulates was complete. In many metal matrix composite systems involving dissimilar materials, an interphase zone has been observed to form, especially when melting and solidification are a means for producing these materials [7]. The reaction zone defining the WC particulate edge formed as titanium from the melt diffused into the WC particulate. This zone is narrow in most cases, but it does alter the chemistry of the WC particulate surface. In the TiC-injected sample, because the dissolved species was the same as the major element in the base alloy, no interphase zone formed at the particulate/ melt interface, nor was there any reason for a reaction zone to form on the TiC particulate surface. Hence, the interface between the particulate and the metal matrix is defined by the unalloyed TiC phase on one side and the solidified Ti–6Al–4V alloy matrix on the other side. However, dendritic and eutectic carbide phases did form from the carbon saturated melt. In the WC-injected Ti–6Al–4V sample, the observed porosity is spherical in nature which suggested a gaseous product released during solidification. Its origin is not known, especially because it was not observed in the TiC-injected sample, nor in the previous work done with the Inconel 625 alloy [5].

These microstructural developments in carbide-injected Ti–6Al–4V alloy were similar to those observed in carbide-injected Inconel 625 alloy [5]. In that work, similarly distributed dendritic and eutectic carbides were found in the WC- and TiC-injected Inconel 625 alloy samples. An interphase zone was found around the carbide particulate in the WC-injected Inconel 625 alloy sample, but none around the carbide particulate in the TiC-injected Inconel 625 alloy sample. However, no reaction zone was observed in the particulate phase in the WC-injected sample. A greater degree of microstructural modification is apparent in the WC-injected sample compared to the TiC injected sample. One reason for this is the lower stability of WC (free energy of formation, $-\Delta F$ at 1500°C of 8.4 kcal mol^{-1}) compared to TiC (39.5 kcal mol^{-1}) [3].

Exposure to natural, flowing sea water had no adverse effect on the Ti–6Al–4V base alloy nor on the TiC-injected surface layer, at least over the exposure period of 1 mon. Detailed microstructural analysis revealed no evidence of corrosion in these samples. There was no crevice corrosion at the sample/epoxy mount boundary in either sample which would have

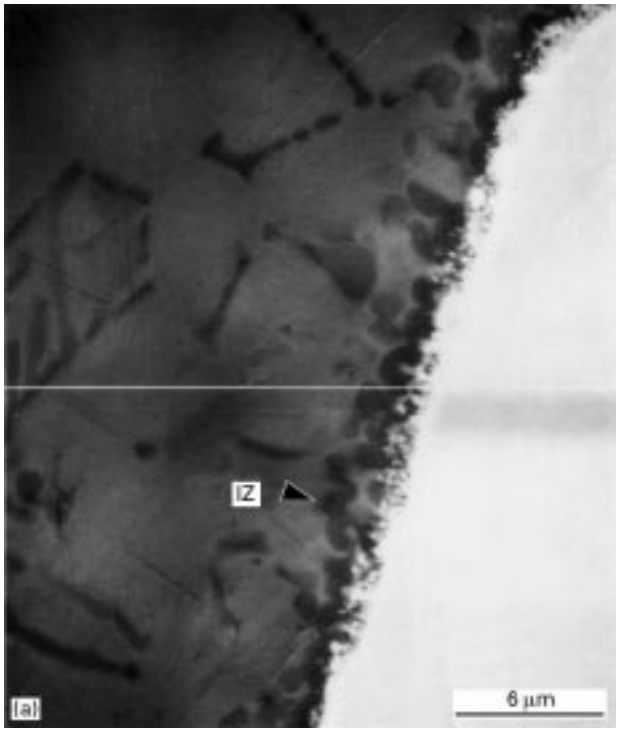

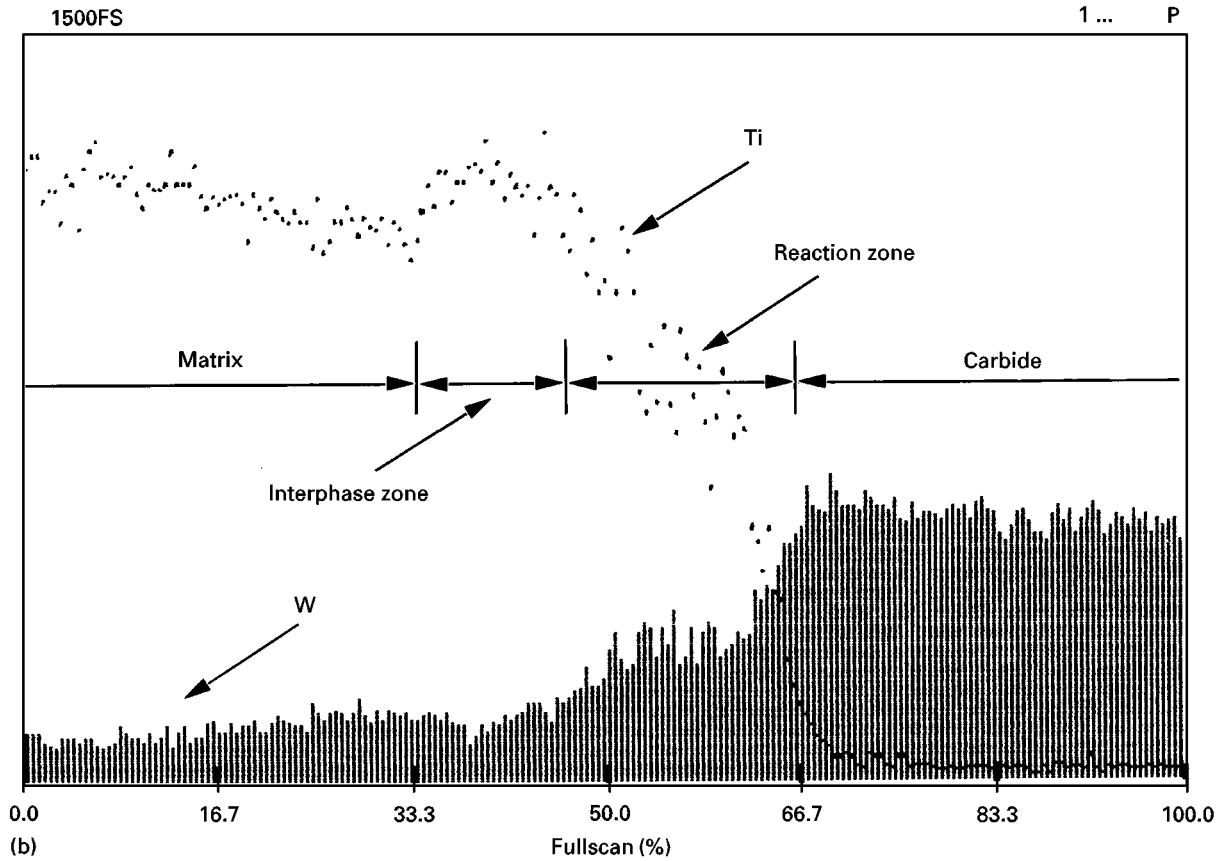

Figure 5 (a) Microstructure showing the cellular–dendritic nature of the interphase zone (IZ) in the WC-injected sample. (b) Corresponding line scan showing increased titanium and lowered tungsten in the IZ.

inhibited other sites from corrosion. However, the WC-injected layer showed corrosion, but only within the WC particulate phase. These results are different from those obtained with Inconel 625 reported earlier [5]. In WC-injected Inconel 625, corrosion of the WC particulate occurred to a much lesser degree, even though it was exposed to sea water for 6 mon compared to 1 mon for the WC injected Ti–6Al–4V. While entire WC particles were corroded away in the Ti–6Al–4V alloy sample, the WC particles in the Inconel 625 alloy sample showed only roughening of the exposed cross-section. Another difference is that corrosion also

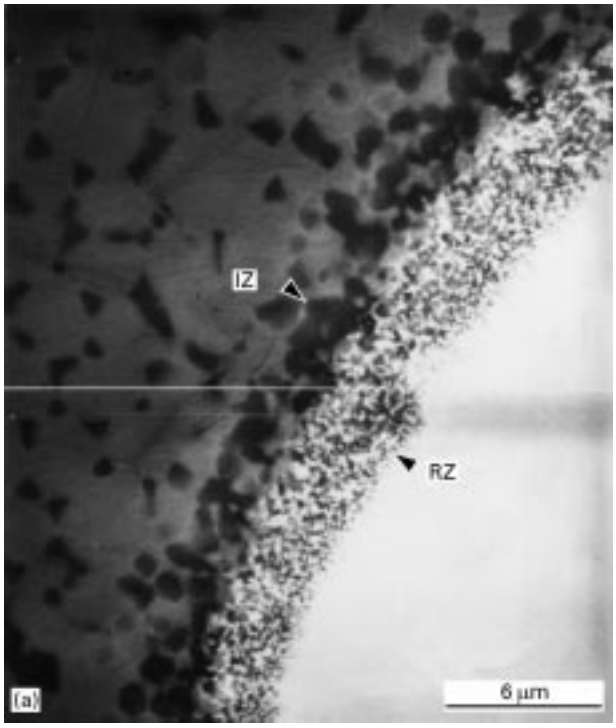

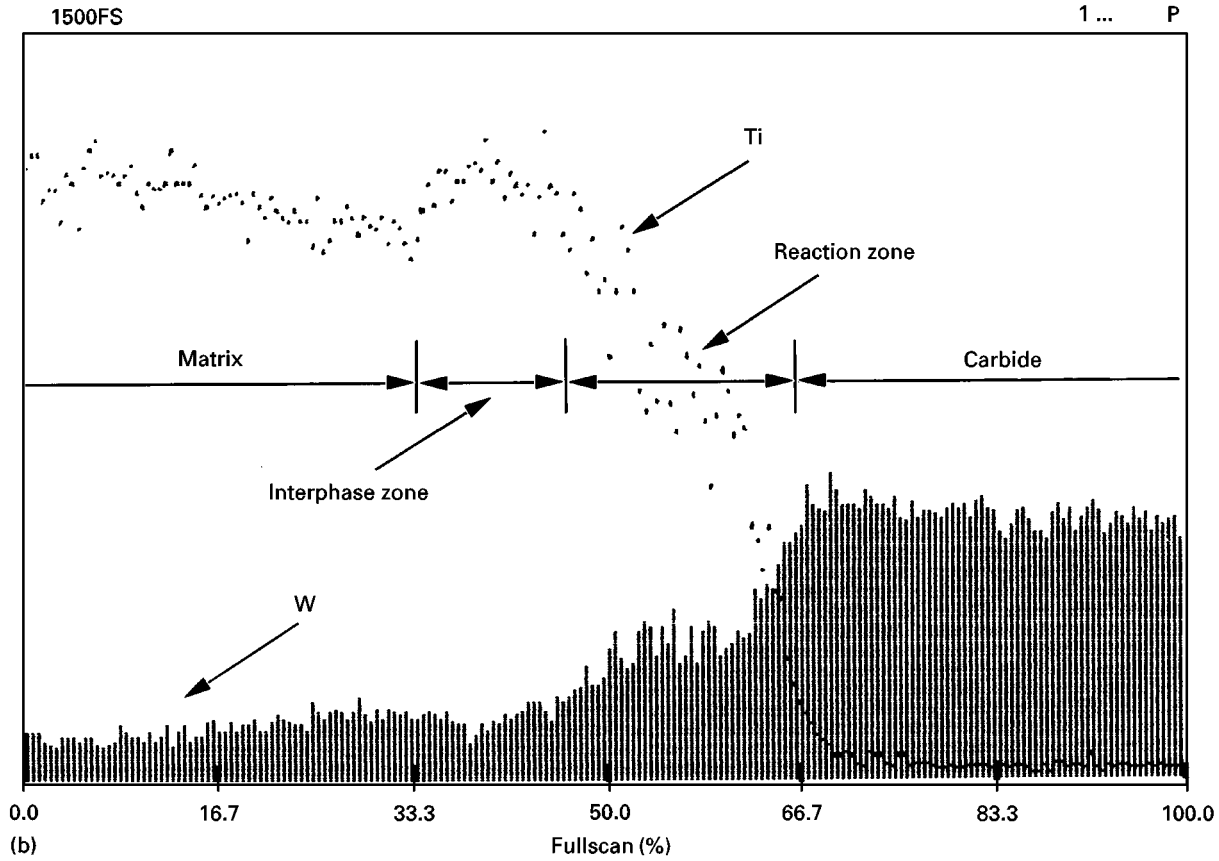

Figure 6 (a) Microstructure showing the interphase zone (IZ) and reaction zone (RZ) in the WC-injected sample. (b) Corresponding line scan showing increased titanium in the IZ and titanium infiltration in the RZ.

occurred in or near the eutectic and dendritic carbides within the Inconel 625 alloy matrix. No corrosion was observed in or adjacent to the eutectic or dendritic carbides in the Ti–6Al–4V alloy matrix in either injected sample. Either the exposure time of 1mon was insufficient to initiate corrosion in these regions or no galvanic couples formed. It is likely that, because the eutectic and dendritic carbides were titanium rich, their electrochemical response was similar to that of the Ti–6Al–4V alloy matrix and no galvanic microcells formed. Neither the alloying of the WC-injected matrix phase with tungsten nor the slight enrichment of the TiC injected matrix with titanium changed the corrosion response of the matrix phase to seawater.

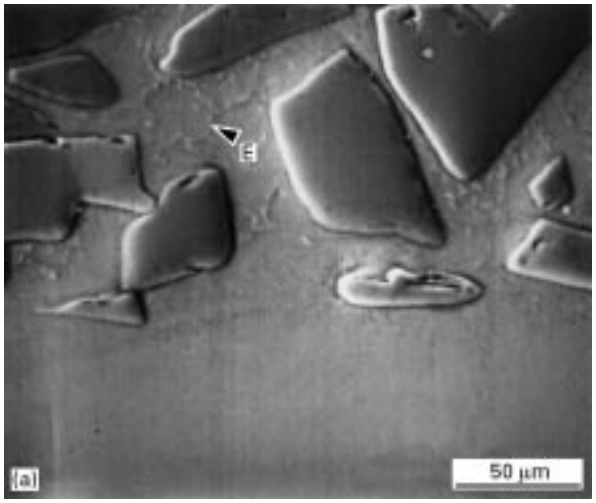

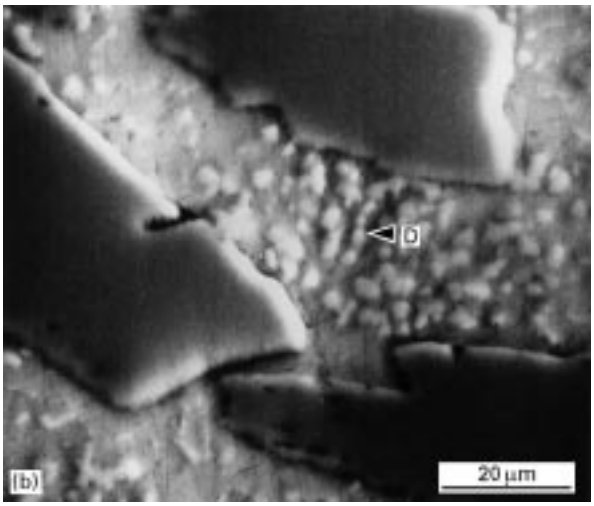

Figure 7 (a) Substrate/injected layer interface in the TiC-injected sample showing cellular structure in the metal matrix with intercellular eutectic (E). (b) Dendritic phase (D) found in the metal matrix in the upper regions of the injected layer.

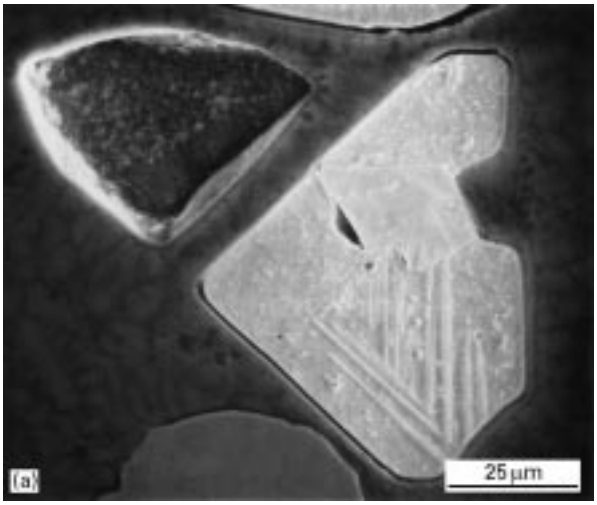

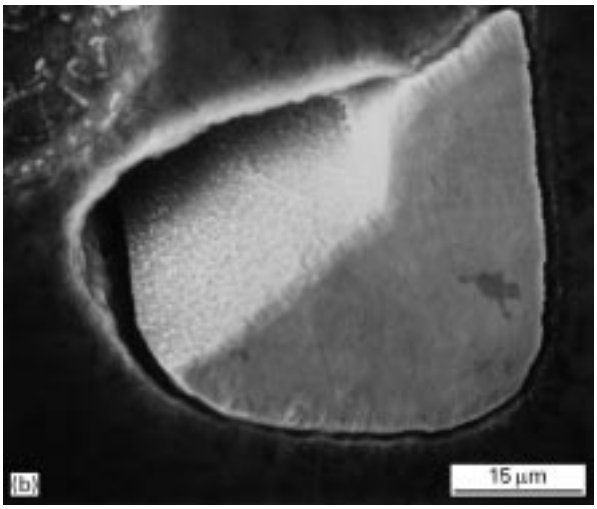

Figure 9 Microstructures showing varying levels of corrosion observed within the WC particulate phase. (a) Surface roughening of the particle on the right, dissolution of entire particle on top left. Note the absence of a reaction zone along the edge of the particle. (b) Partial dissolution of a particle.

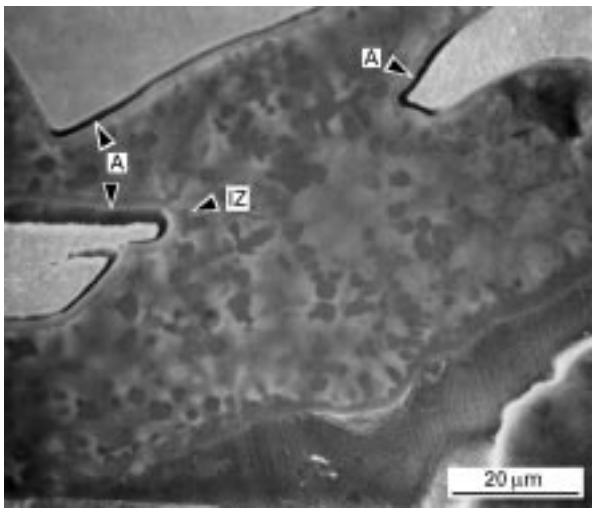

Figure 8 Microstructure showing crevice-type corrosion (A) at the carbide particulate (C) /interphase zone (IZ) interface in the WC-injected sample. Note the absence of corrosion in the cellular matrix, or in or near the eutectic.

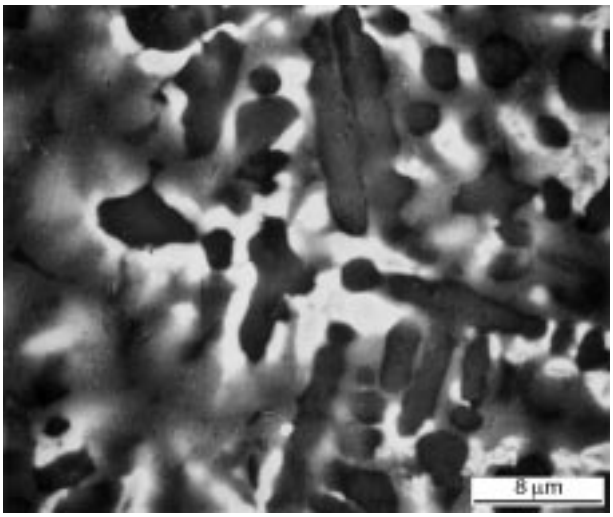

Figure 10 Microstructure showing the absence of corrosion in the dendritic regions of the metal matrix in a WC-injected sample.

The matrix phase remained corrosion resistant as did the base metal and the HAZ. Also, no corrosion was observed in or near the porosity in the WC-injected sample. This suggests that by whatever process the pore formed, no product phase resulted that would have caused corrosion.

Because the most severe corrosion attack was at the interface between the WC particulate and the

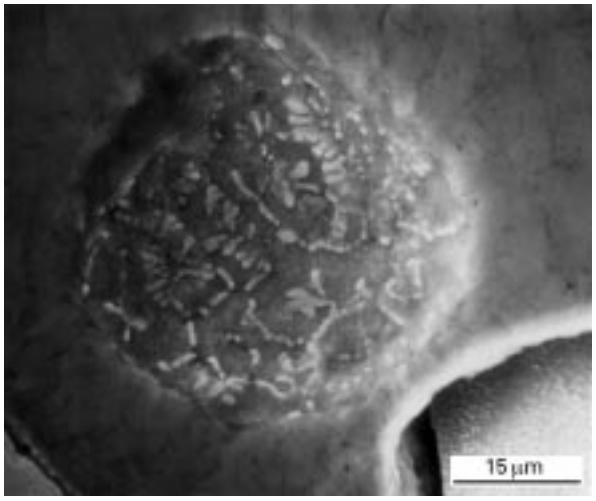

Figure 11 Microstructure showing inter-cellular eutectic in a pore in the WC-injected sample, but the absence of corrosion in or around it.

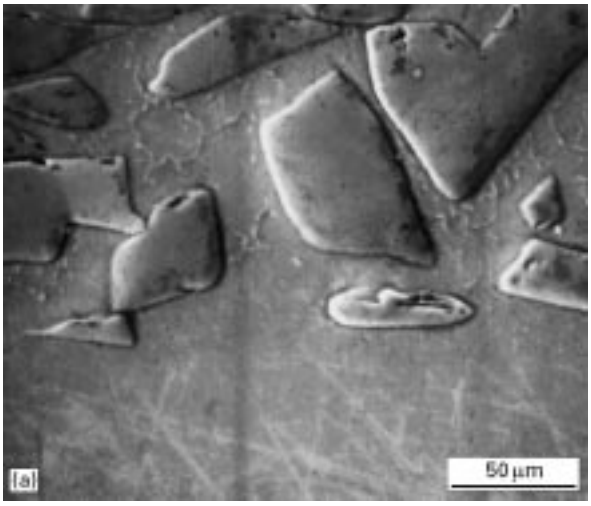

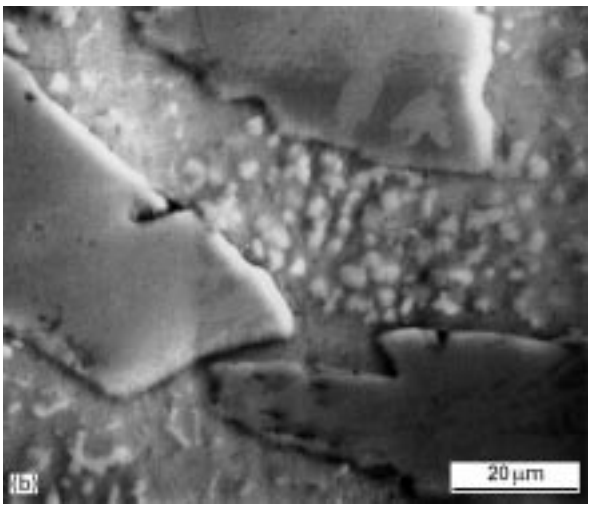

Figure 12 (a) Substrate/injected layer interface in a TiC-injected sample, showing no corrosion in the cellular structure nor in or near the intercellular eutectic. (b) Upper regions of the injected layer showing no corrosion in the dendritic phase in the metal matrix.

interphase zone, a galvanic couple must have formed between these two phases. The WC phase became the anode and the titanium rich interphase zone became the cathode. While most of the WC particles in the

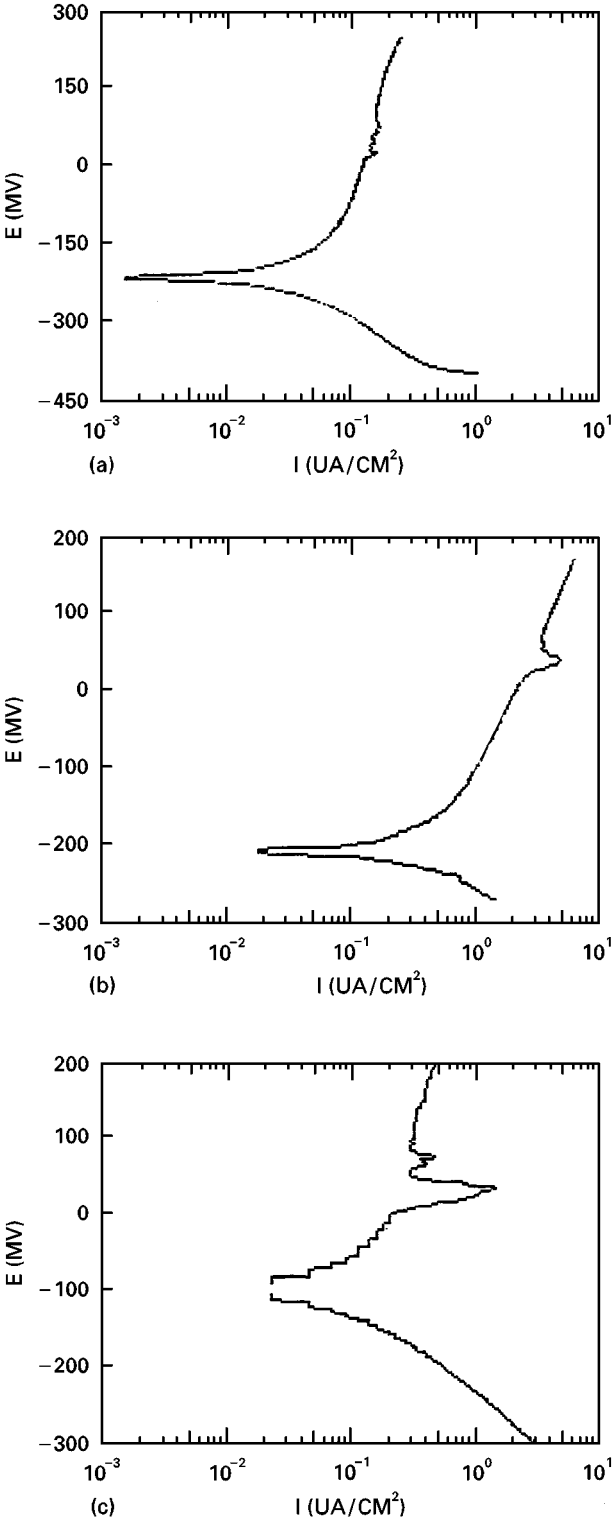

Figure 13 Electrochemical polarization scans (a) Ti–6Al–4V base alloy. (b) The WC injected layer. (c) The TiC injected layer.

TABLE II Corrosion rates in carbide-injected Ti–6Al–4V alloy samples

Sample	Corrosion rate (mil y^{-1})[a]	
	Polarization resistance	Tafel analysis
Ti–6Al–4V	0.24	0.06
TiC-injected	0.03	0.00
WC-injected	0.62	0.63

[a] 1 mil = 2.54×10^{-5} m.

injected layer showed attack, some particles were more severely attacked than others. Some showed modest roughening of the exposed surface, some were corroded halfway, and others were entirely consumed. This variation in corrosion rate from one particle to another may be related to the particle size and to its crystallographic orientation to the corrosion media. Smaller particles and particles with favourable orientation would be more severely attacked. Alternatively, it could be related to variations in the strength of the galvanic cells. Regardless of the severity of the attack across the particulate, all WC particulates that were surrounded by an interphase zone experienced strong crevice corrosion at the interphase zone/particulate interface. The same behaviour was observed in WC-injected Inconel 625 alloy [5], but the severity of attack in the WC particulate was much less and that may be related to a less strong galvanic couple in the WC/Inconel 625 system. Another reason why accelerated corrosion occurred into the WC particulate may be the existence of the titanium infiltrated reaction zone in the particulate's surface. Because crevice corrosion was observed to have started in this reaction zone, it suggests that it was probably the most active site for corrosion. The fact that a reaction zone already existed in the as-cast structure prior to corrosion testing may indicate the beginning of the formation of a galvanic couple between the interphase zone and the WC particulate. In fact that it appears pitted may support this analysis.

The sea water corrosion mechanism may be explained by the sequence of stages schematically presented in Fig. 14. In this diagram, a slice perpendicular to the sea water exposed polished surface is considered. In stage 1, a galvanic couple forms between the WC particulate and the titanium-rich interphase zone. In stage 2, crevice corrosion begins at the interface between the particulate and interphase zone, proceeds along this interface and through the reaction zone into the WC particulate. At the same time, corrosion begins across the exposed polished surface of the particulate phase, making it appear rough. Corrosion at the interface occurs at a faster rate than corrosion of the carbide surface because the ion exchange is most rapid at the interface and less rapid away from it. In stage 3, corrosion proceeds at a rapid rate in both directions, along the interface and across the carbide surface. If this process is not halted, e.g. by removing the sample from sea water, in stage 4, the entire particle ends up being consumed leaving behind a cavity.

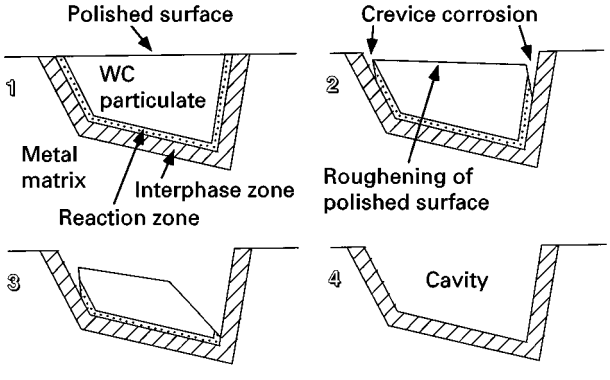

Figure 14 A possible mechanism for the corrosion of the particulate phase during sea water corrosion of WC-injected Ti–Al–4V alloy sample.

The corrosion behaviour of these materials is related to both the nature of the particulate/metal matrix galvanic couple as well as the overall resistivity of the particulate material itself. Binary carbides do not appear in the galvanic series in sea water reported by Baboian and Pohlman [8]. It is not known whether WC and TiC are more noble than the Ti–6Al–4V alloy in an aqueous medium, but both WC and TiC are insoluble in most acids, alkali solutions and salt solutions [9,10] and are unaffected by sea water. Corrosion data given in ASM Handbook Vol. 13 show that all three materials have high resistance to corrosion in sea water [11]. The WC particulate with a resistivity of 17 $\mu\Omega$ cm is more conductive than the TiC particulate, which has a resistivity 60–250 $\mu\Omega$ cm [8]. Because the interphase zone surrounding the WC particulate is a titanium-rich carbide, its properties are probably similar to those of TiC and, hence, it is more insulating than WC. The resulting galvanic reaction and the better conductivity of the anodic WC would likely cause the observed corrosion WC particulate phase and the observed increase in the corrosion rate in the WC-injected sample. Although Ti–6Al–4V with a resistivity of 0.0171 $\mu\Omega$ cm and TiC are far apart in their resistivities, no galvanic couple formed between them in the injected layer. We have not determined the exact reason for this behaviour. It is possible that because both phases have titanium as the major element, they may be very close in the galvanic series. Another reason may be passivation early in the testing process. Passivation and other processes may also have precluded corrosion in and near the eutectic and dendritic carbides and within the alloyed metal matrix.

Overall, the measured corrosion rates were relatively small for all specimens. However, the WC-injected specimen showed a significantly higher corrosion rate as compared to both the base material and the TiC injected specimen. In actual service, these rates would likely be greater because the cathode to anode surface area ratios invariably would be increased. Of the corrosion rate calculations performed, the Ti–6Al–4V base material showed the least agreement between the two techniques. Calculations using the polarization resistance method involved relating the corrosion rate to the inherent resistive properties of the material in the corrosive electrolyte. This may contribute to the uncertainty in the measurement.

In addition to the corrosion rate data, the polarization scans for the TiC- and WC-injected samples show the presence of a secondary anodic reaction. The value of the secondary reaction anodic current for the WC specimen (3 $\mu A\,cm^{-2}$) was increased by approximately an order of magnitude over that for the TiC specimen (0.3 $\mu A\,cm^{-2}$). This secondary anodic feature was not noted in the corresponding data for the Ti–6Al–4V base material and may be related to the composite nature of the exposed surface of the injected

layers. The significance of the secondary anodic reaction is not currently known, other than that it is clearly related to the presence of the metal matrix/particulate injected layer above the Ti–6Al–4V base material. More experimental work is currently underway to identify the exact nature of the polarization behaviour of the injected materials. The behaviour of the overall WC anodic polarization suggests the tendency for increased galvanic attack and greater corrosion. These data are consistent with the measured corrosion rates and the visual observations discussed previously.

No corrosion work involving metal matrix composites of WC and TiC with Ti–6A1–4V has been found in the literature and definitely none on wear-resistant composite surfaces. Most of the previous work on sea water corrosion in metal matrix composites involved SiC or graphite particulate- or fibre-reinforced aluminium magnesium alloys [12]. In most cases, if corrosion was observed, it occurred as a pitting phenomenon in the metal matrix surrounding the reinforcement such as observed in aluminium surrounding the SiC particulate [13]. This corrosion was related to the formation of a galvanic couple between the particulate and the metal matrix with the metal becoming anodic. Corrosion of the carbide particulate was not observed. These results are different from our observations in which corrosion occurred in the particulate phase but not in the metal matrix in spite of microstructural inhomogeneities resulting from complex solidification reactions.

5. Conclusion

A variety of microstructural features was identified in carbide-injected Ti–6Al–4V alloy samples. The general structure of the injected layer was a metal matrix/carbide particulate composite. The metal matrix had a cellular structure and was modestly alloyed with the metal portion of the injected carbides. Within the metal matrix were found eutectic and dentritic carbides, and in the case of WC, an interphase zone around the particulate and a reaction zone within the surface of the particulate were found. Sea water corrosion studies showed corrosion in the WC-injected specimen but none in the TiC-injected specimen after 1 mon exposure. Corrosion in the WC-injected sample was confined to the particulate phase and was directly a result of the presence of the interphase zone. The interphase zone was found to be rich in titanium with characteristics similar to TiC. Having a lower resistivity than TiC, the WC particulate formed the anodic side of a galvanic couple with the interphase zone. Corrosion appeared to begin at the interface between the interphase zone and the WC particulate. It quickly proceeded into the reaction zone on the WC surface and, depending upon the size and crystallographic orientation of the particulates, portions or all of the WC particulate were observed to be consumed. None of the other solidification products were locations for corrosions. Corrosion rate measurements confirmed the microstructural observations on sea water-exposed specimens.

References

1. C. W. DRAPER and P. MAZZOLDI (eds), Laser Surface Treatment of Metals (Martinus Nijhoff, Dordrecht, The Netherlands 1986.)
2. K. P. COOPER, in "Friction, Lubrication and Wear Technology", ASM Handbook Vol. 18, edited by P. J. Blau (ASM International, Materials Park, OH, 1992) p. 861.
3. *Idem*, in "Laser Beam Surface Treating and Coating", Vol. 957, edited by G. Sepold (SPIE, Bellingham, WA, 1988) p. 42.
4. K. P. COOPER and J. D. AYERS, in "Laser Surface Modification", edited by F. D. Seaman (AWS, Miami, FL, 1988) p. 115.
5. K. P. COOPER, P. SLEBODNICK and E. D. THOMAS, *Mater. Sci. Eng.* **A206** (1996) 138.
6. "Properties and Processing Ti–6Al–4V", Technical Publication (TIMET, Pittsburgh, PA, 1986) p. 8.
7. P. ROHATGI, in "Casting" Metals Handbook, Vol. 15, 9th Edn, edited by D. M. Stefanescu (ASM International, Materials Park, OH, 1988) p. 840.
8. R. BABOIAN and S. L. POHLMAN, in "Corrosion", Metals Handbook, Vol. 13, 9th Edn, edited by L. J. Korb and D. L. Olson (ASM International, Materials Park, OH, 1987) p. 83.
9. D. R. LIDE (ed.), "Handbook of Chemistry and Physics", 75th Edn (CRC Press, Boca Raton, FL, 1994) pp. 4–108.
10. E. K. STORMS, "Refractory Carbides" (Academic Press, New York, NY, 1986).
11. "Corrosion", Metals Handbook, Vol. 13, 9th Edn, edited by L. J. Korb and D. L. Olson (ASM International, Materials Park, OH, 1987) pp. 677, 850.
12. L. H. HIHARA and R. M. LATANISION, *Int. Mater. Rev.* **39** (1994) 245.
13. D. M. AYLOR and R. M. KAIN, in "Recent Advances in Composites in the United States and Japan", ASTM STP 864, edited by J. R. Vinson and M. Taya (American Society for Testing and Materials, Philadelphia, PA, 1985) p. 632.

Received 30 October 1997
and accepted 15 May 1998